The catalytic thermo-oxidative decomposition of glimepiride using the isoconversional method

Najamus Sahar Riyaz[1] · Ismail Badran[1]

Abstract

Applying the isoconversional method to data obtained from thermogravimetric analysis (TGA) can provide vital kinetic information. In this work, the thermal decomposition and oxidation of the antidiabetic drug glimepiride is analyzed in the presence of N_2 and O_2. The study was done with and without metal oxide catalysts to explore their potential application in solid wastewater upgrading. The analysis was conducted using thermogravimetric analysis. The isoconversional methods of Kissinger–Akahira–Sunose and Friedman were used to estimate the effective activation energies as a function of the extent of conversion (α). Density functional calculations were used to estimate the bond dissociation energies in glimepiride. The E_a values obtained from the Friedman method and the DFT calculations indicate an initial S–N bond breaking in glimepiride. The pre-exponential factor (A) and the kinetic triplet ($\Delta H^{\ddagger}$, $\Delta S^{\ddagger}$, and $\Delta G^{\ddagger}$) are also discussed. When glimepiride oxidation was studied in the presence of the metal oxides, the catalyst activity was found to follow the order $VO_2 > CuO > MnO_2 > Al_2O_3 > TiO_2$.

Keywords Pharmaceutical · Thermogravimetric analysis · Catalysts · Isoconversional · Adsorption · Oxidation

Introduction

Fresh water supplies across the globe face major concerns due to a new class of micropollutants, such as pharmaceutical and personal care products (PPCP) [1–3]. Such pollutants can pose high risks to human health as well as animal life [1, 4, 5]. PPCP enter the aquatic environments mainly through human activities. This includes body excretion, waste disposed from sewage treatment plants (STPs), landfill leaching sites along wastewater treatment plants (WWTP), as well as hospitals and factories [5–8]. In fact, WWTP are considered the primary source of water contamination by PPCP because they were not originally designed to treat such pollutants [5–7, 9].

Among several technologies that were developed recently to treat PPCP pollution, adsorption rises as one of the most efficient, economic, and feasible techniques [3, 10–12]. However, conventional adsorption is challenged by the fact that it returns solid wastes concentrated on the adsorbent surface because of the water treatment process [13, 14]. To resolve this problem, a new technology was recently developed to utilize the adsorbent as a catalyst for further upgrading of the solid waste [10, 13–16]. Under specific conditions, the nanoadsorbent, commonly a metal oxide, would catalyze the conversion of the solid wastes into useful chemicals or fuel. The term *nanosorbcat* (Scheme 1) was coined to describe this technology. The upgrading of the solid waste can proceed by thermal decomposition, air oxidation, partial oxidation by steam, or light photolysis. The nanoadsorbent then can be recycled for further treatment cycles.

Metal oxides are one of the most prominent nanoadsorbents [10, 12, 17]. The concept of nanosorbcats relies on developing a nanocatalyst that is commercially available, non-toxic, easy to recycle and transport, and highly effective [18]. It is thus primitive to study the upgrading mechanisms shown in Scheme 1 to comprehend and optimize the function of nanosorbcats. This can be done by several methods including thermogravimetric analysis (TGA). Recently, we studied the neat thermal degradation of metformin [19], a common diabetes drug, as well as its thermal oxidation [20]. Our studies showed that metformin wastes can be converted into ammonia and nitrogen-rich small molecules that can

✉ Ismail Badran
  ibadran@qu.edu.qa

1 Department of Chemistry and Earth Sciences, College
   of Arts and Sciences, Qatar University, P.O. Box: 2713,
   Doha, Qatar

Scheme 1 The concept of nano-sorbcat
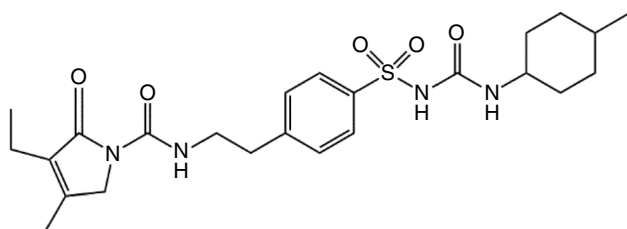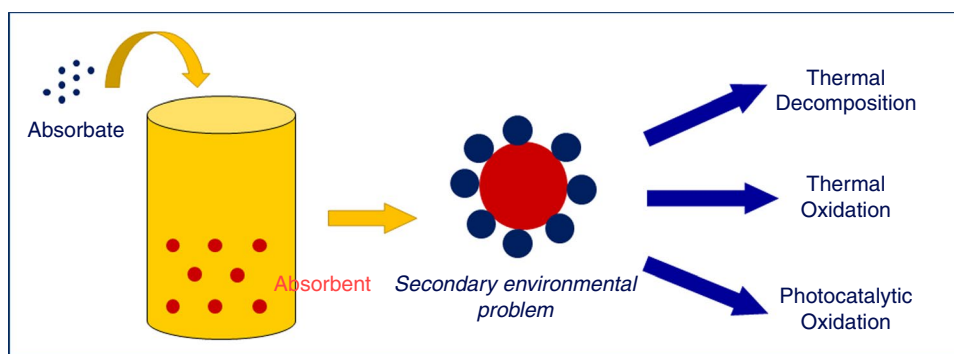
Scheme 2 Molecular structure of glimepiride

be utilized as industrial building blocks. Both studies were done in the absence of catalyst to set a benchmark or future studies. As a continuation to our efforts, this work is done in the presence of a group of metal oxide catalysts in order to evaluate their catalytic behavior, and potential use as nanosorbcats.

Glimepiride (Amaryl) was chosen as a model PPCP molecule due to its wide use in treating type II diabetes [21, 22]. The presence of glimepiride (GPD, Scheme 2) in wastewater can cause harm to human or animal health. Overdoses of GPD can lead to disastrous effects such as hypoglycemia and, in severe cases, even lead to prolonged hospitalization [23–25]. In addition, GPD is not completely metabolized by the human body and can thus make its way into the WWTP. The removal of GPD from wastewater was studied using multi-walled carbon nanotubes (MWCNT) [21]. The study showed that GPD can mostly be removed from aqueous media using MWCNT in a continuous-flow setup.

In this work, both the thermal degradation (under inert atmosphere) and the thermal oxidation (under O_2) of GPD were studied using TGA. The thermo-oxidative decomposition was also studied in the presence of different metal oxide catalysts. The isoconversional methods of Kissinger–Akahira–Sunose (KAS) and Friedman (FR) were implemented to construct the reaction mechanism and obtain the kinetics parameters. These methods can avoid the drawbacks of conventional model-fitting methods because they make no assumptions about the reaction model and allow the activation energy to be determined as a function of the degree of

conversion (α) [26]. Further analysis was also done to determine the pre-exponential factor (A) and the kinetic triplet ($\Delta H^{\ddagger}$, $\Delta S^{\ddagger}$, and $\Delta G^{\ddagger}$). Quantum theoretical calculations were also implemented to help explain the reaction mechanism of GPD degradation and correlate the theoretical activation energies with those obtained experimentally.

Experimental

Materials

Glimepiride (99.0%, M.Wt. 490.62 g mol^{-1}) was obtained from Alfa Aesar (Tewksbury, MA, USA). Vanadium Oxide (VO_2, > 98%), Titanium Oxide (TiO_2, > 98%), Aluminum Oxide (Al_2O_3, > 98%), Manganese Oxide (MnO_2, > 98%), and Copper Oxide (CuO, > 98%) were obtained from Sigma-Aldrich Chemical Company (Milwaukee, Wisconsin, USA). Zirconium Oxide (ZrO_2, 99%) was obtained from Riedel-de Haën GmbH (Seelze, Germany). All chemicals were used as received. N_2 gas (5.0) and O_2 (4.8) gases were obtained from National Industrial Gas Plants, Doha, Qatar.

Thermogravimetric analysis (TGA)

The TGA experiments on GPD were done using a digital TGA analyzer (SDT Q600, TA Instruments, Delaware, USA). The experiments were done in two phases. First, the analysis was done under N_2 environment to obtain the kinetic parameters for the neat thermal decomposition of the drug. Next, the experiments were performed under O_2 with and without the metal oxide catalysts. The analysis was observed at different heating rates in the range of 5–30 °C min^{-1}.

In a typical experiment, 10 mg of GPD were weighted and transferred into a clean dried pan. The sample was heated under a consent gas flow of 20 cm^3 min^{-1} from room temperature to 120 °C and hold at that temperature for 10 min. to remove any misroute, before heating continues to the desired temperature (~ 800 °C). After each experiment, the machine was left to cool down to room temperature and the pan was

cleaned with 1.0 M HNO_3. For the catalyzed experiments, the 10-mg GPD were gently mixed with the desired amount of the metal oxide until obtaining homogenous mixture. The following oxides were tested: ZnO, CuO, MnO_2, TiO_2, ZrO_2, Al_2O_3, and VO_2. The selection of the catalysts was based on their common use and high activity in the chemical industry. The results of ZnO were omitted because the oxide was observed to decompose at high temperatures.

The mass loss and the derivative mass as a function of temperature were recorded for each experiment and analyzed using OriginPro 2020 [27].

Theoretical calculations

The exact details of the theoretical calculations involved in this work are described in previous studies [2, 19, 28]. In brief, the molecular structures of GPD and the expected fragments from the thermal decomposition were optimized using the density functional MN12L [29] along with the $6-31+G(d,p)$ basis set. Frequency calculations were requested after each successful optimization at the same level of theory to ensure the validity of each structure. The calculations of the enthalpy, entropy, and Gibbs free energies involved in this work can be found elsewhere [2, 19, 28]. All calculations were done using Gaussian 16 Rev C.01 [30] and viewed using Gaussview. [31]

Isoconversional analysis

Isoconversional methods are referred to as model-free methods as they allow the analysis of reaction dynamics and determining parameters of the reaction such as activation energy (E_α) without prior evaluation of the reaction model [32, 33]. These methods can calculate the activation energy of the reaction conducted at multiple heating rates, provided that all other parameters are kept constant [19, 20, 32, 33]. The principle of isoconversional methods is based on the statement that the rate of any mechanism or process at constant increments of conversion is only a function of temperature [32, 33]. This principle can be further utilized to determine the isoconversional values of the activation energy of the process. This temperature dependence can only be utilized when the reaction is conducted at four to five different temperatures or heating rates.

Two types of isoconversional methods, the Kissinger–Akahira–Sunose (KAS) and Friedman (FR), were conducted on the sets of data. The primary objective of using these analyses is to determine the activation energy for the different steps of the decomposition mechanism.

The Friedman method is one of the first reported isoconversional methods and is based on the following equation [34]:

$$ln\left(\beta_i \frac{d\alpha}{dT}\right) = -\frac{E_\alpha}{RT_i} + \ln(A_\alpha f(a)) \tag{1}$$

where α is the degree of conversion and is given by:

$$\alpha = \frac{m_0 - m}{m_0 - m_f} = \frac{\Delta m}{\Delta m_{tot}} \tag{2}$$

where m_0 is the initial sample mass, m_f is the final mass and m is the mass at a given time.

In Eq. (1), β_i represents the heating rate and is defined as $\beta_i = dT/dt$ for linear non-isothermal reaction [35]. The index (i) corresponds to various temperature programs, T_i is the temperature at which the degree of conversion (α) is achieved under the corresponding heating rate. By this, the term $\ln(A_\alpha) + \ln f(\alpha)$ remains unchanged for a given (α). Thus, E_α can be estimated from the slope of the best fitting of the plot $\ln(\beta_i \frac{d\alpha}{dT})$ vs. $\left(\frac{1}{T_i}\right)$ [34]:

The KAS method is based on the following equation [36].

$$\ln\left(\frac{\beta_i}{T_{\alpha,i}^2}\right) = \ln\left(-\frac{A_\alpha R}{E_\alpha}\right) - \ln g(\alpha) - \left(\frac{E_\alpha}{RT_{\alpha,i}}\right) \tag{3}$$

where $g(\alpha)$ is the integral form of the reaction model ($f(\alpha)$). Hence, the effective activation energies can be estimated from the plot of the left side of Eq. (3) against $1/T_{\alpha,i}$ at a given α.

Using the previously calculated values of dm/dt, the value of $\frac{d\alpha}{dT}$ was calculated using the equation below:

$$\frac{d\alpha}{dT} = \frac{-dm/dt}{m_0 - m_f} \tag{4}$$

This equation generates a set of $\frac{d\alpha}{dT}$ values with temperatures corresponding to different αs. Subsequently, E_α was determined from the slope of the linear plot between the calculated values of $\ln \beta/T^2$ and the corresponding values of temperature found in the previous steps of the analysis. These values of E_α were then plotted against the values of α to represent the isoconversional analysis.

Results and discussion

Thermal decomposition of GPD under N_2

The neat thermal decomposition of GPD was investigated under inert N_2 atmosphere. Figure 1 shows the curves of GPD in the temperature range 100–800 °C at different heating rates of 5, 10, and 20 °C min^{-1}. The decomposition of GPD starts around 200 °C and is associated with several mass losses. Meanwhile, the derivative thermogravimetry (DTG) curve shows two peaks at around 210 and 290 °C.
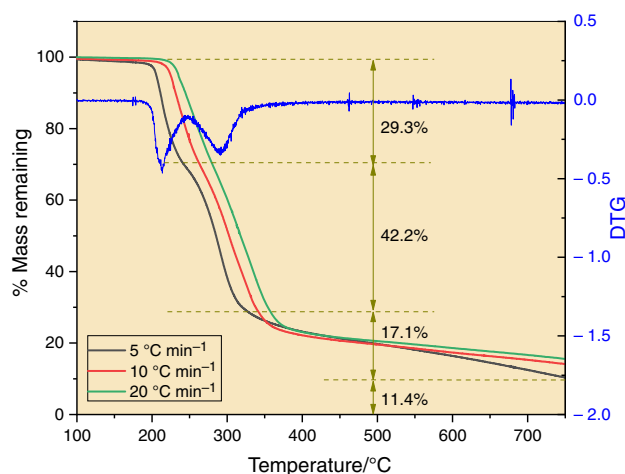
Fig. 1 TGA curve for GPD thermal decomposition at nitrogen flow of 20 mL min^{-1} and different heating rates. The red line represents the derivative mass at heating rate of 5 °C min^{-1}. (For clarification of the color in this figure, the reader is referred to the web version of this article)

The first peak corresponds to the quick melting of GPD which has a reported melting point of 207 °C [37].

The first mass loss is estimated at 29.3% and correlates with a strong DTG peak. Because the experiment is done under inert atmosphere, this is considered an endothermic transition since no oxidation is involved [36]. To account for this mass loss, we implemented quantum theoretical calculations to construct a possible mechanism for GPD decomposition. Scheme 3 shows three different possible pathways of GPD degradation obtained from breaking the bonds labeled b, c, and e. According to our calculations, the S–N bond (b) is the weakest bond with an estimated dissociation energy of 238.8 kJ mol^{-1}. The rupture of this bond leads to the formation of fragment I, which has a molecular mass equivalent to 29.3% out of the total mass of GPD. This agrees very well with the first mass loss at 210 °C in GPD as shown in Fig. 1.

Scheme 3 also shows the dissociation energies of bonds a to f in GPD. Apparently, they are all higher than that of bond b. In a study by Bansal et al. using LC–MS [38], the neutral forms of II and III were suggested as possible products of GPD alkaline hydrolysis. An unknown product was also mentioned in Bansal's study, but its exact structure was not determined. Based on our calculations, we suggest that the neutral form of I might be a result of GPD alkaline hydrolysis as well as its thermal decomposition.

The next mass loss in GPD takes place at around 290 °C and is associated with another endothermic peak as shown in Fig. 1. This loss, estimated at 42.2% is due to further degradation of fragment 1. Under our experimental conditions, GPD does not completely degrade up to a high temperature of 800 °C, and around 10–15% (depending on the heating rate) are left unreacted (*cf.* Fig. 1).

## Kinetics of the thermal decomposition

The kinetics of the thermal decomposition of GPD was analyzed using the isoconversional method as illustrated in the experimental section. This method describes the reaction rate (dα/dt) as a function of temperature and the state of the reaction mixture [20, 35]. The method allows the calculation of the activation energy (E_α) as a function of the extent of conversion (α) over a narrow temperature range. The method was developed to treat heterogeneous reactions that involves multiple steps [20, 35].

Figure 2 shows the isoconversional kinetics for GPD decomposition at four different heating rates. As shown, the decomposition is shifted gradually to higher temperature by increasing the heating rate, and the isoconversional curves are well separated for α between 0 and 0.75. This allows the evaluation of E_α as described by Eqs. (1–4). Figure 3 depicts the Arrhenius plots for this reaction using the FR method. Excellent linear fittings were obtained where α is between 0 and 0.75, in agreement with the isoconversional analysis of Fig. 2. Similar Arrhenius plots were also obtained using the KAS method. By applying Eqs. 1 and 3, the corresponding E_α values were obtained from the slopes of the Arrhenius fittings, and they are depicted as a function of α in Fig. 4.

The results of Fig. 4 demonstrate a variation of E_α as the extent of the conversion increases. This is because each E_α value is correlated to a single reaction step within a complex reaction mechanism [20, 32, 33]. This is the advantage of using isoconversional methods, such as FR and KAS, to describe complex reactions that involves solid/gas heterogenous interactions. In addition, Fig. 4 shows that the E_α values obtained by the FR method are higher than those obtained by KAS. This observation was evident in previous studies [20, 39]. The FR values range between *ca.* 150–300 kJ mol^{-1}, while those obtained by KAS are between 90 and 110 kJ mol^{-1}. We noted that the calculated theoretical E_a value for breaking the S–N bond (b) in GPD (*cf.* Scheme 3) is 238.8 kJ mol^{-1}, which lies in the range of the experimental E_α values obtained by the FR method. In our recent work on the thermo-oxidative decomposition of metformin, [20] we concluded that FR method is more reliable in obtaining E_α values as it provides values close to that obtained by DFT calculations. The result of this work reinforces this conclusion.

The experimental E_a values derived by FR method, at $\alpha > 0.5$, are slightly higher than the theoretical value of breaking bond b. This is because the theoretical values are calculated under ambient conditions, *i.e.*, 1 atm, 298 K. However, the experimental conditions of our work are not the same as standard conditions and the thermal decomposition is conducted at much higher temperatures, resulting in values with variable differences.

Scheme 3 Thermal decomposition of glimepiride as constructed by theoretical calculations. Energies represent enthalpies changes at 298 K for homolytic bond dissociations obtained at MN12L/6–31 + G(d,p) level of theory
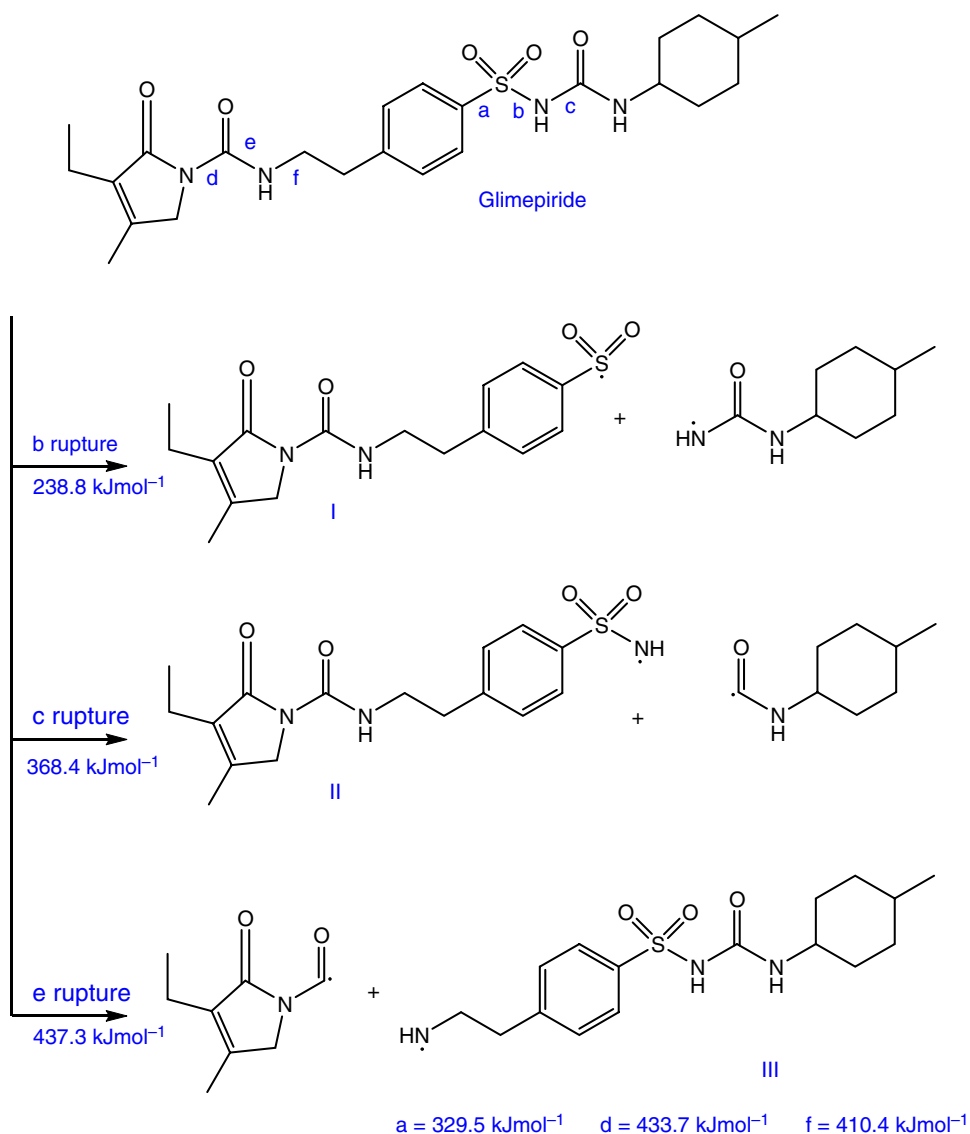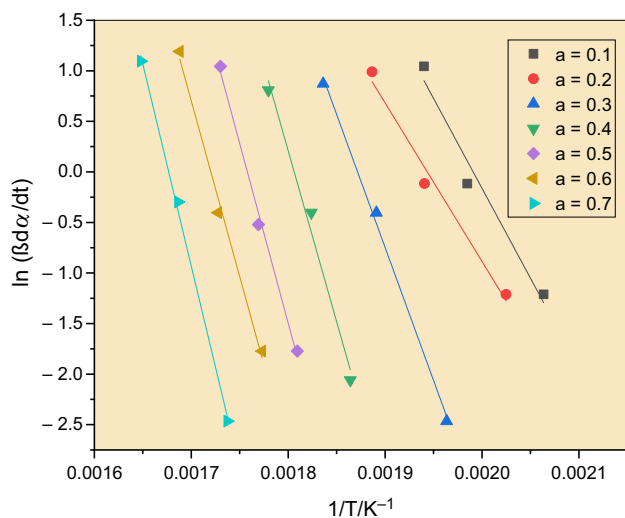

Oxidation of GPD under O2

The oxidation of GPD was investigated using thermogravimetry under a constant flow of O_2 gas. The TGA curves for GPD oxidation at six different heating rates are shown in Fig. 5. The figure also shows the derivative mass curve at 5 °C min^{-1}. The diagram starts with thermal decomposition in the low temperature region, 200–500 °C, with two DTG peaks in accordance with thermal decomposition (Fig. 1) In the presence of O_2, a third DTG peak is observed around 545 °C, with further mass loss of GPD. This is mostly due to its oxidation at that temperature. As shown in the figure, the thermo-oxidative decomposition of GPD is divided into four regions, quick melting around 210 °C, thermal decomposition between 210 and 320 °C, an overlap region between 320 and 500 °C, and oxidation between 500 and 600 °C. In contrast to the neat thermal decomposition in Fig. 1, the

oxidative decomposition of GPD is complete by 620 °C and no mass is left in the crucible, indicating complete oxidation. Over the overlap region, the reaction mechanism becomes more complicated, as the reaction transforms from thermal decomposition into oxidation involving several initiation primary reactions [19, 20].

The isoconversional analysis was done for GPD oxidation and it is shown in Fig. 6. The effective activation energies (E_α) of oxidation were determined for the whole range except those lying within the overlap region, $0.55 < \alpha < 0.7$, where the isoconversional method is not applicable [20, 32, 33]. The Arrhenius plots at different extents of conversion (α) for the oxidation of GPD are shown in Fig. 7. The gap in the middle of the figure is due to the overlap region where the estimated energies (E_α) where not reliable as mentioned earlier. Figure 8 shows the estimated experimental E_α values obtained from the slope of the Arrhenius plots using the FR
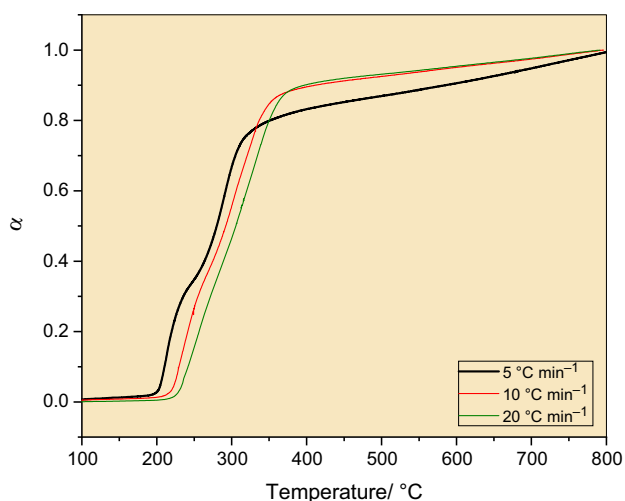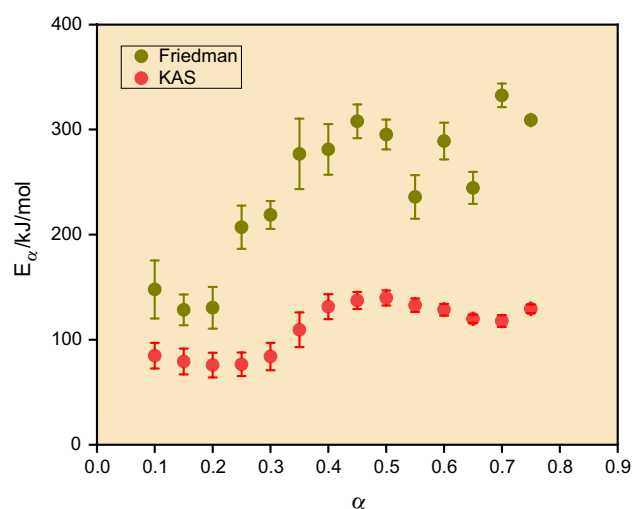
Fig. 2 The extent of conversion (α) as a function of temperature at different heating rates under N_2 of 20 mL min^{-1} for the GPD thermal decomposition

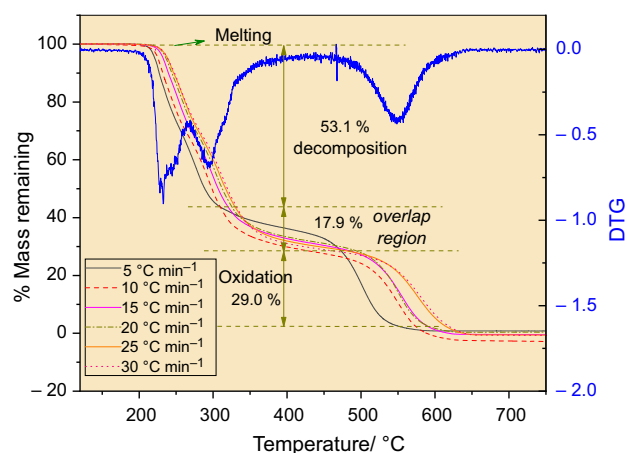**Fig. 4** Dependence of the activation energy E_α as function of the extent of conversion (α) for the thermal decomposition of GPD in N_2 between 180 and 750 °C using the FR and KAS methods
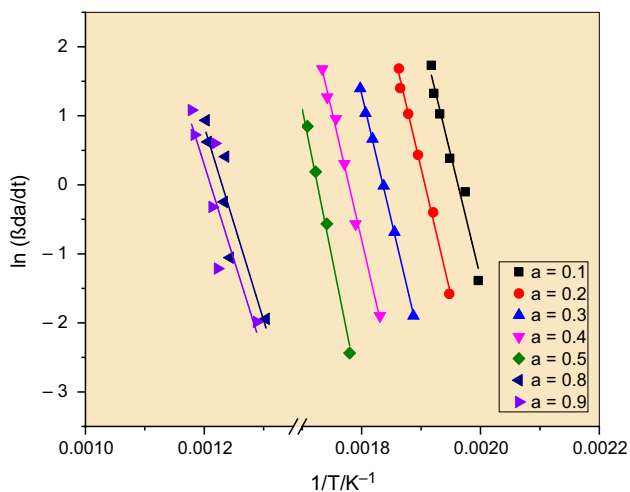

Fig. 3 Arrhenius plots for the thermal decomposition of GPD in N_2 between 180 and 750 °C using the FR method

Fig. 5 TGA curve for GPD oxidation under oxygen flow of 20 mL min^{-1} and different heating rates. Red line represents the derivative mass at heating rate of 5 °C min^{-1}. (For clarification of the color in this figure, the reader is referred to the web version of this article)

and KAS methods. The values obtained from FR are relatively higher as explained earlier. Up to $0.5 < \alpha$, the E_α values are around 300 kJ mol^{-1}, which is close to those obtained from the thermal decomposition as discussed in Sect. 3.2. As the reaction progress, the E_α values decrease at elevated temperatures. This is because as the reactive mass decreases and the molecule becomes more fragmented, it becomes more susceptible to oxidation at higher temperatures [20, 40, 41].

Oxidation of organic molecules is a complex process where several oxygenated species are involved in the reaction mechanism [42]. Such species include molecular oxygen (O_2), hydroxyl (OH) hyperoxo (O_2^-), peroxo (ROO) and mono oxygen atoms (O). In our recent work on metformin

[20], we used theoretical calculations to estimate the activation energies for oxidation reactions initiated by oxygen (O_2) as well as atomic oxygen (O), both in their *triplet* ground states. We concluded that metformin oxidation is more likely to be ruled by O_2 attacks rather than single O atoms due to the high bond dissociation energy of O_2 required to generate O atoms [20]. In this work, the E_α values obtained using the FR method between $0.75 < \alpha < 0.95$ are in the range of 200–300 kJ mol^{-1}. In the current work, the Eα values obtained under the FR method (between $0.75 < \alpha < 0.95$) were determined to be in the range of 200–300 kJ mol^{-1}.
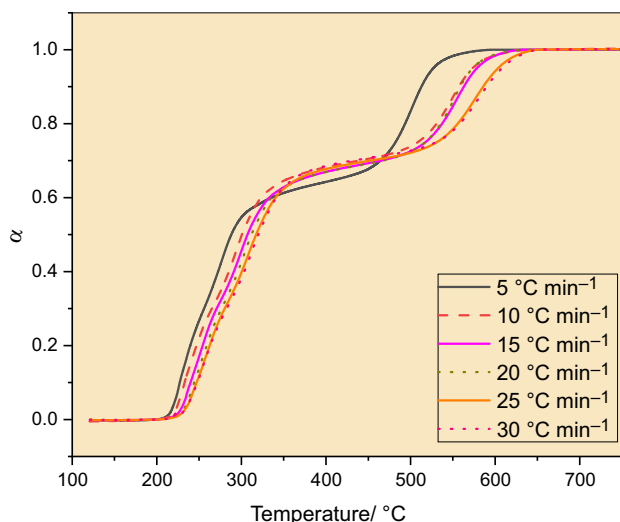
Fig. 6 GPD oxidation showing the extent of conversion (α) as a function of temperature at different heating rates. O_2 airflow = 20 mL min^{-1}

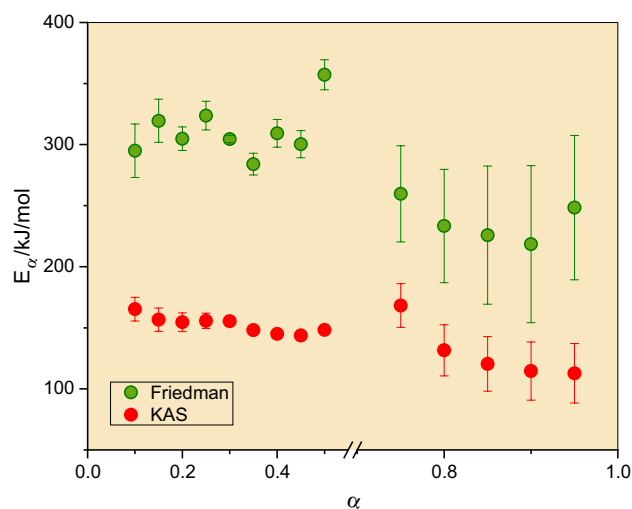**Fig. 8** Dependence of the activation energy E_α as function of the extent of conversion (α) for the oxidation of GPD in O_2 between 180 and 750 °C using the FR and KAS methods

Fig. 7 Arrhenius plots for the oxidation of GPD in O_2 between 180 and 750 °C using the FR method

The calculated theoretical Gibbs free energies of activation ($\Delta G^{\ddagger}$) for O_2 attacks on metformin [20] have aslo ranged between 200–300 kJ mol^{-1}. Therfore, we suggest that GPD oxidation is most likely to proceed by O_2 attacks, similar to metformin.

Kinetic modeling and determination of the kinetic triplet

The isoconversional method can be used to determine the reaction model and subsequently the kinetic parameters, A, $\Delta H^{\ddagger}$, $\Delta S^{\ddagger}$, and $\Delta G^{\ddagger}$. Using the Friedman equation (Eq. 1), one can plot the left side of Eq. 1 ($\ln(\beta_i \frac{d\alpha}{dT}$ against $\ln f(\alpha)$ for some

known models of $f(\alpha)$. The slope of the linear fitting should be unity according to Eq. 1 [32, 33]. Using the experimental data for GPD reactions under both N_2 and O_2, we applied this fitting to different reaction models as proposed earlier [32, 33]. The results of the linear fittings are shown in Tables S1 and S2 in the supplementary information section. Although we attempted the fittings at different values of α, the best results were obtained for $\alpha = 0.25$. The best fitting was obtained for the three-dimensional diffusion model represented by:

$$f(a) = 3/2(1 - \alpha)^{2/3}\left[1 - (1 - \alpha)^{1/3}\right]^{-1} \tag{5}$$

Since the y-intercept of the linear fitting is equal to $\ln(A_\alpha f(a))$, the values of the pre-exponential factor A_α were calculated by substituting the values $f(a)$ intercept into the intercepts.

The unimolecular pre-exponential factor (A_α) is defined as [43]:

$$A_{uni} = \left(\frac{ek_BT}{h}\right)e^{\Delta S^{\neq}/R} \tag{6}$$

where e is the Napier's constant (2.7183), k_B is Boltzmann constant, h is Planck's constant, and R is the universal gas constant. Therefore, it is possible to rearrange Eq. 6 to obtain the entropy of activation, $\Delta S^{\neq}$ [20, 43]:

$$\Delta S^{\neq} = R\left(\ln\frac{Ah}{ek_BT}\right) \tag{7}$$

Furthermore, the enthalpy ($\Delta H^{\neq}$) and the Gibbs free energy ($\Delta G^{\neq}$) of activations can be obtained from the following relationships [43]:

$$E_a = \Delta H^{\neq} + RT \tag{8}$$

$$\Delta G^{\neq} = \Delta H^{\neq} - T\Delta S^{\neq} \tag{9}$$

The results of this kinetic analysis are tabulated in Table 1. The A_α values at 25% conversion are equal to 2.8×10^{19} and 3.5×10^{30} s^{-1} for the reactions under N$_2$ and O$_2$, respectively. The physical meaning of the pre-exponential factor can be understood from its definition in Eq. 6. Higher value of A_α leads to a higher $\Delta S^{\neq}$. This is indeed reflected by the values of $\Delta S^{\neq}$ obtained at 114.7 and 327.0 J mol^{-1} K^{-1}.

In Sect. 3.1, we explained the GPD thermal decomposition in N$_2$ to be mostly caused by a neat S–N bond rupture. Thus, the $\Delta S^{\neq}$ for this step is most likely related to a transition state with an elongated S–N bond, and its structure does not much differ than that of GPD. This is what is referred to by a *tight* transition state. Under O$_2$, more *loose* transition states are expected as a result of oxygen attacking GPD that initiates its oxidation. This can explain the large difference between $\Delta S^{\neq}$ values under N$_2$ or O$_2$ in this work. Table 1 also shows the values of $\Delta H^{\neq}$ and $\Delta G^{\neq}$ under the same conditions. The $\Delta H^{\neq}$ value under O$_2$ (319.4 kJ mol^{-1}) is much higher than that under N$_2$ (202.8 kJ mol^{-1}) because it depends on the experimental E_a according to Eq. 8. However, the values of $\Delta G^{\neq}$ are very close. According to Eq. 9, $\Delta G^{\neq}$ depends on both $\Delta H^{\neq}$ and $\Delta S^{\neq}$. Because of the high value of $\Delta S^{\neq}$ under O$_2$, the term $-T\Delta S^{\neq}$ becomes smaller causing a $\Delta G^{\neq}$ close to that of N$_2$ reactions. Finally, the value of $\Delta H^{\neq}$ related to GPD decomposition under N$_2$ is estimated at 202.8 kJ mol^{-1}. This is close to the bond dissociation energy (238.8 kJ mol^{-1}) for S–N obtained by DFT in Sect. 3.1.

Catalytic oxidation of GPD

The effect of adding a catalyst on GPD oxidation was studied by mixing different metal oxides with GPD powder before each experiment. This was done to examine the catalytic activity of these metal oxides and their potential use as nanosorbcats, as detailed in Scheme 1. All experimental conditions were kept like the uncatalyzed reactions for the sake of fair comparison. Figure 9 depicts the TGA curves obtained after mixing 6 metal oxides, namely: CuO, MnO$_2$,
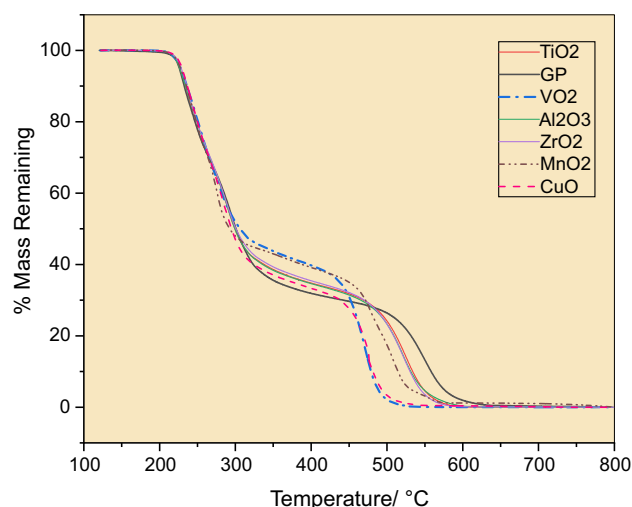
Fig. 9 The catalyzed thermo-oxidative decomposition of GPD under O$_2$ flow of 20 mL min^{-1} at 10 °C min^{-1} in the presence of several metal oxides

TiO$_2$, ZrO$_2$, Al$_2$O$_3$, and VO$_2$, with GPD. The ratio of the metal oxide to GPD was kept at 10% for all experiments. The results of this study demonstrate different catalytic activity for the examined catalysts. In the first decomposition zone, up to 300 °C, the TGA curves are not highly affected by the addition of a catalyst. This is a reasonable observation because thermal decomposition of organic compounds does involve simple homolytic bond dissociation and should not be highly affected by the addition of a catalyst. However, in the next oxidation zone, between 450 and 600 °C, the effect of adding a catalyst is clear. For every metal oxide, the TGA curve has been shifted to lower temperature from the uncatalyzed curve (red dashed line). The shift from the uncatalyzed curve reflects the catalytic activity and therefore its efficiency. Thus, the catalytic efficiency observed in this can be described by:

$$VO_2 > CuO > MnO_2 > Al_2O_3 > TiO_2$$
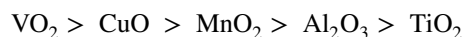
The catalytic activity is also illustrated by the shift of the DTG peaks as shown in Fig. 10. Within the first decomposition region, the two DTG peaks for the pure GPD at 210 and 300 °C are not largely affected by the presence of

Table 1 Kinetic parameters obtained by combining Friedman equation with model fitting at $a = 0.05$

Conditions	T/°C	$f(\alpha)$	Slope	R^2	A_α/s^{-1})	$\Delta S^{\ddagger}$J mol^{-1} K^{-1}	$\Delta H^{\ddagger}$/kJ mol^{-1}	$\Delta G^{\ddagger}$/kJ mol^{-1}
Under N$_2$	227	$3/2(1-\alpha)^{2/3}$ $[1-(1-\alpha)^{1/3}]^{-1}$	1.35	0.9887	$2.8 10^{19}$	114.7	202.8	145.5
Under O$_2$	248		2.24	0.9960	$3.5 10^{30}$	327.0	319.4	149.1
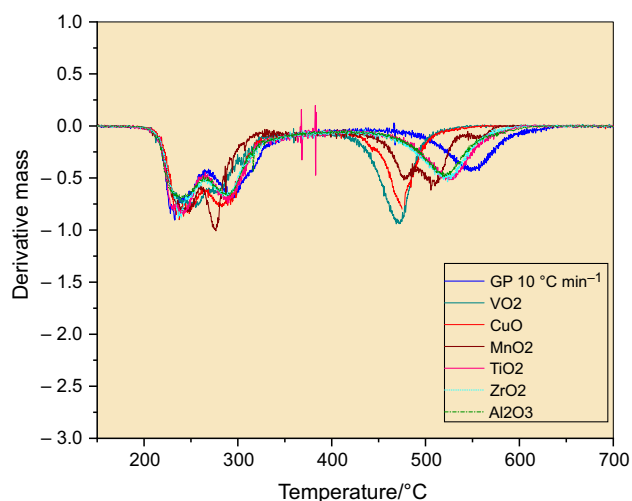
Fig. 10 DTG curves for thermo-oxidative decomposition of GPD under O_2 flow of 20 mL min^{-1} at 10 °C min^{-1} in the presence of several metal oxides
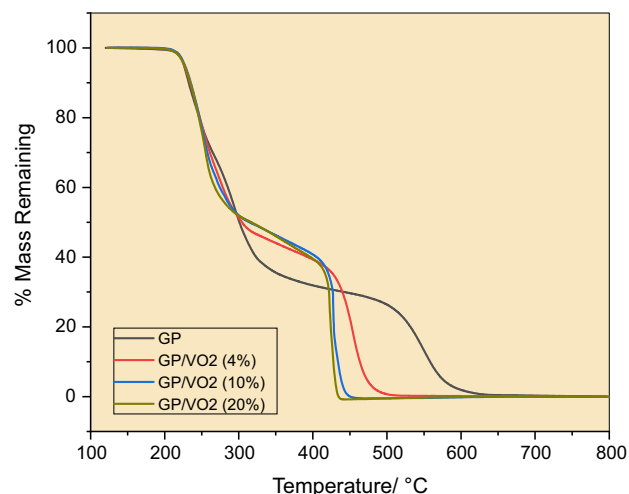
Fig. 11 Effect of adding different amounts of catalyst on the thermo-oxidative decomposition of GPD under O_2. Flow rate = 20 mL min^{-1}, Heating rate = 10 °C min^{-1}

the metal oxide. However, the third DTG peak at 550 °C is largely shifted to the left in the presence of the catalyst. The best catalysts, VO_2, caused the oxidation to start at around 490 °C, sixty degrees Celsius lower than that of the pure compound.

To further investigate the catalytic effect on the oxidation of GPD. The effect of the amount of catalyst was studied using VO_2 as illustrated in Fig. 11. Three different ratios of 4, 10, and 20% VO_2 were tested and shown along with the original experiment conducted without the presence of vanadium oxide. As the amount of catalyst increases, the TGA curve is shifted towards lower temperatures within the

oxidation zone, indicating that VO_2 is indeed acting as a catalyst.

As mentioned in the introduction, this work was done to explore the potential use of the metal oxides as nanosorbcats. The results obtained in this section demonstrate that the tested metal oxides can catalyze the thermal oxidation of glimepiride. VO_2 and CuO, which are known to be good adsorbents, can be used to catalyze the oxidation of GPD, and possibly similar pollutants. This can be used to develop a complete solution for the adsorptive removal of organic pollutants, where the catalyst can be recycled, and leaving no solid sludge.

Conclusions

This project investigated the thermal decomposition and oxidation of glimepiride, a common antidiabetic drug, using thermogravimetric analysis under N_2 and O_2 as well as with various catalysts. It was revealed that under N_2 atmosphere there were two significant mass losses corresponding to stepwise thermal degradation of the drug. Theoretical calculations revealed that the degradation was initiated with an S–N bond rupture followed by further degradation. The effective activation energies (E_α) for the reaction were estimated using the isoconversional methods of Kissinger–Akahira–Sunose (KAS) and Friedman (FR). The E_α values obtained by FR method were ranged between 150 and 300 kJ mol^{-1}and they were considered more reliable as they better match the theoretical values.

Using the FR isoconversional method, the data were best to a dimensional diffusion reaction model (f_α). The model was then used to determine the pre-exponential factors (A_α), which then used to determine the kinetic triplet $\Delta H^{\ddagger}$, $\Delta S^{\ddagger}$, and $\Delta G^{\ddagger}$. The final values of $\Delta G^{\ddagger}$ indicate higher barriers for GPD oxidation that its thermal decomposition.

Under O_2 atmosphere, a third mass loss around 540 °C was observed and attributed to the oxidation of the drug. Using the FR isoconversional method, the E_α values for the oxidation zone were ranging around 200 kJ mol^{-1}.

The thermogravimetric analysis was then performed in the presence of few metal oxide catalysts, and it was evident that the oxides were able to catalyze the oxidation of GPD, but not its thermal decomposition. The catalyst efficiency of the metal oxides was found to follow the order $VO_2 > CuO > MnO_2 > Al_2O_3 > TiO_2$.

The outcomes of this study are crucial for the future development of a nanoadsorbent that can act as an adsorbent and a catalyst (nanosorbcat). Such material can overcome the problems of conventional adsorption, by

allowing the effective degradation and removal of GPD and other drugs from wastewater streams.

Data availability All data generated or analysed during this study are included in this published article [and its supplementary information files].

Declarations

Conflict of interest The authors declare that they have no competing interests. The authors declare that there is no conflict of interest regarding the publication of this article.

References

1. Wang J, Wang S. Removal of pharmaceuticals and personal care products (PPCPs) from wastewater: a review. J Environ Manage. 2016;182:620–40. https://doi.org/10.1016/j.jenvman.2016.07.049.
2. Badran I, Manasrah AD, Nassar NN. A combined experimental and density functional theory study of metformin oxy-cracking for pharmaceutical wastewater treatment. RSC Adv. 2019;9(24):13403–13. https://doi.org/10.1039/C9RA01641D.
3. Almanassra IW, Kochkodan V, Ponnusamy G, McKay G, Ali Atieh M, Al-Ansari T. Carbide derived carbon (CDC) as novel adsorbent for ibuprofen removal from synthetic water and treated sewage effluent. J Environ Health Sci Eng. 2020;18(2):1375–90. https://doi.org/10.1007/s40201-020-00554-0.
4. Ebele AJ, Abou-Elwafa Abdallah M, Harrad S. Pharmaceuticals and personal care products (PPCPs) in the freshwater aquatic environment. Emerg Contam. 2017;3(1):1–16. https://doi.org/10.1016/j.emcon.2016.12.004.
5. Kibuye FA, Gall HE, Elkin KR, Ayers B, Veith TL, Miller M, et al. Fate of pharmaceuticals in a spray-irrigation system: from wastewater to groundwater. Sci Total Environ. 2019;654:197–208. https://doi.org/10.1016/j.scitotenv.2018.10.442.
6. Mackuľak T, Černanský S, Fehér M, Birošová L, Gál M. Pharmaceuticals, drugs, and resistant microorganisms — environmental impact on population health. Curr Opin Environ Sci Health. 2019;9:40–8. https://doi.org/10.1016/j.coesh.2019.04.002.
7. Couto CF, Lange LC, Amaral MCS. Occurrence, fate and removal of pharmaceutically active compounds (PhACs) in water and wastewater treatment plants—a review. J Water Process Eng. 2019;32: 100927. https://doi.org/10.1016/j.jwpe.2019.100927.
8. Prichard E, Granek EF. Effects of pharmaceuticals and personal care products on marine organisms: from single-species studies to an ecosystem-based approach. Environ Sci Pollut Res. 2016;23(22):22365–84. https://doi.org/10.1007/s11356-016-7282-0.
9. Bradley PM, Journey CA, Button DT, Carlisle DM, Clark JM, Mahler BJ et al. Metformin and other pharmaceuticals widespread in wadeable streams of the southeastern United States. Environ Sci Technol Lett. 2016;3(6):243–9. https://doi.org/10.1021/acs.estlett.6b00170
10. Badran I, Khalaf R. Adsorptive removal of alizarin dye from wastewater using maghemite nanoadsorbents. Sep Sci Technol. 2019;55(14):2433–48. https://doi.org/10.1080/01496395.2019.1634731.
11. Abbas H, Manasrah AD, Saad AA, Sebakhy KO, Bouhadda Y. Adsorption of Algerian asphaltenes onto synthesized maghemiteiron oxide nanoparticles. Pet Chem. 2021;61(1):67–75. https://doi.org/10.1134/S0965544121010072.
12. Borji H, Ayoub GM, Bilbeisi R, Nassar N, Malaeb L. How effective are nanomaterials for the removal of heavy metals from water and wastewater? Water Air Soil Pollut. 2020;231(7):330. https://doi.org/10.1007/s11270-020-04681-0.
13. El-Qanni A, Nassar NN, Vitale G. A combined experimental and computational modeling study on adsorption of propionic acid onto silica-embedded NiO/MgO nanoparticles. Chem Eng J. 2017;327:666–77. https://doi.org/10.1016/j.cej.2017.06.126.
14. Marei NN, Nassar NN, Hmoudah M, El-Qanni A, Vitale G, Hassan A. Nanosize effects of NiO nanosorbcats on adsorption and catalytic thermo-oxidative decomposition of vacuum residue asphaltenes. Can J Chem Eng. 2017;95(10):1864–74. https://doi.org/10.1002/cjce.22884.
15. Alnajjar M, Hethnawi A, Nafie G, Hassan A, Vitale G, Nassar NN. Silica-alumina composite as an effective adsorbent for the removal of metformin from water. J Environ Chem Eng. 2019;7(3): 102994. https://doi.org/10.1016/j.jece.2019.102994.
16. El-Qanni A, Nassar NN, Vitale G, Hassan A. Maghemite nanosorbcats for methylene blue adsorption and subsequent catalytic thermo-oxidative decomposition: computational modeling and thermodynamics studies. J Coll Interface Sci. 2016;461:396–408. https://doi.org/10.1016/j.jcis.2015.09.041.
17. Védrine JC. Metal oxides in heterogeneous oxidation catalysis: state of the art and challenges for a more sustainable world. Chem Sus Chem. 2019;12(3):577–88. https://doi.org/10.1002/cssc.201802248.
18. Salih KSM, Mamone P, Dörr G, Bauer TO, Brodyanski A, Wagner C, Kopnarski M, Taylor RNK, Demeshko S, Meyer F, Schünemann V, Ernst S, Gooßen LJ, Thiel WR. Facile synthesis of monodisperse maghemite and ferrite nanocrystals from metal

powder and octanoic acid. Chem Mater. 2013;25:1430–1435. https://doi.org/10.1021/cm303344z

19. Badran I, Hassan A, Manasrah AD, Nassar NN. Experimental and theoretical studies on the thermal decomposition of metformin. J Therm Anal Calorim. 2019;138(1):433–41. https://doi.org/10.1007/s10973-019-08213-9.

20. Badran I, Manasrah AD, Hassan A, Nassar NN. Kinetic study of the thermo-oxidative decomposition of metformin by isoconversional and theoretical methods. Thermochim Acta. 2020. https://doi.org/10.1016/j.tca.2020.178797.

21. Badran I, Qut O, Manasrah AD, Abualhasan M. Continuous adsorptive removal of glimepiride using multi-walled carbon nanotubes in fixed-bed column. Environ Sci Pollut Res. 2020. https://doi.org/10.1007/s11356-020-11679-y.

22. Gangji AS, Cukierman T, Gerstein HC, Goldsmith CH, Clase CM. A systematic review and meta-analysis of hypoglycemia and cardiovascular events: a comparison of glyburide with other secretagogues and with insulin. Diabetes Care. 2007;30(2):389–94. https://doi.org/10.2337/dc06-1789.

23. Kiran T, Shastri N, Ramakrishna S, Sadanandam M. Surface solid dispersion of glimepiride for enhancement of dissolution rate. Int J Pharm Tech Res. 2009;1(3):822–31.

24. Jasim SM, Baban RS, Jasim HS. Adsorption of glimepiride on activated charcoal and Iraqi kaolin from aqueous solution. Iraqi J Med Sci. 2013;11(1):24–32.

25. Saudek CD, Derr RL, Kalyani RR. Assessing glycemia in diabetes using self-monitoring blood glucose and hemoglobin A1c. JAMA. 2006;295(14):1688–97. https://doi.org/10.1001/jama.295.14.1688.

26. Yuan X, He T, Cao H, Yuan Q. Cattle manure pyrolysis process: Kinetic and thermodynamic analysis with isoconversional methods. Renew Energy. 2017;107:489–96. https://doi.org/10.1016/j.renene.2017.02.026.

27. OriginLab Corporation. OriginPro 9.1: Scientific data analysis and graphing software. Northampton, MA, USA2019.

28. Badran I, Rauk A, Shi Y. New orbital symmetry-allowed route for cycloreversion of silacyclobutane and its methyl derivatives. J Phys Chem A. 2019;123(9):1749–57. https://doi.org/10.1021/acs.jpca.8b08071.

29. Peverati R, Truhlar DG. Screened-exchange density functionals with broad accuracy for chemistry and solid-state physics. PCCP. 2012;14(47):16187–91. https://doi.org/10.1039/C2CP42576A.

30. Frisch MJ, Trucks GW, Schlegel HB, Scuseria GE, Robb MA, Cheeseman JR et al. Gaussian 16 Rev. C.01. Wallingford, CT2016.

31. Dennington R, Keith T, Millam J. GaussView, version 5. 2009.

32. Vyazovkin S. Isoconversional kinetics of thermally stimulated processes. New York, NY, USA: Springer; 2015.

33. Vyazovkin S, Burnham AK, Criado JM, Pérez-Maqueda LA, Popescu C, Sbirrazzuoli N. ICTAC Kinetics Committee recommendations for performing kinetic computations on thermal analysis data. Thermochim Acta. 2011;520(1):1–19. https://doi.org/10.1016/j.tca.2011.03.034.

34. Friedman HL. New methods for evaluating kinetic parameters from thermal analysis data. J Polym Sci Part C Polym Lett. 1969;7(1):41–6. https://doi.org/10.1002/pol.1969.110070109.

35. Vyazovkin S, Wight CA. Isothermal and non-isothermal kinetics of thermally stimulated reactions of solids. Int Rev Phys Chem. 1998;17(3):407–33. https://doi.org/10.1080/014423598230108.

36. Cides LCS, Araújo AAS, Santos-Filho M, Matos JR. Thermal-behaviour, compatibility study and decomposition kinetics of glimepiride underisothermal and non-isothermal conditions. J Therm Anal Calorim. 2006;84(2):441–5. https://doi.org/10.1007/s10973-005-7131-8.

37. Lestari MLAD, Indrayanto G. Chapter 5 - Glimepiride. In: Brittain HG, editor. Profiles of drug substances, excipients and related methodology. Academic Press; 2011. p. 169–204.

38. Bansal G, Singh M, Jindal KC, Singh S. LC-UV-PDA and LC-MS studies to characterize degradation products of glimepiride. J Pharm Biomed Anal. 2008;48(3):788–95. https://doi.org/10.1016/j.jpba.2008.08.003.

39. Sbirrazzuoli N, Girault Y, Elégant L. Simulations for evaluation of kinetic methods in differential scanning calorimetry. Part 3 — Peak maximum evolution methods and isoconversional methods. Thermochim Acta. 1997;293(1):25–37. https://doi.org/10.1016/S0040-6031(97)00023-3.

40. Badran I, Nassar NN, Marei NN, Hassan A. Theoretical and thermogravimetric study on the thermo-oxidative decomposition of Quinolin-65 as an asphaltene model molecule. RSC Adv. 2016;6(59):54418–30. https://doi.org/10.1039/C6RA07761G.

41. Narayanaswamy K, Blanquart G, Pitsch H. A consistent chemical mechanism for oxidation of substituted aromatic species. Combust Flame. 2010;157(10):1879–98. https://doi.org/10.1016/j.combustflame.2010.07.009.

42. Schlögl R. Concepts in selective oxidation of small alkane molecules. Modern heterogeneous oxidation catalysis: design, reactions and characterization. Hoboken, NJ, USA: Wiley-VCH Verlag GmbH & Co.; 2009.

43. Atkins PW, De Paula J, Keeler J. Atkins' Physical chemistry. 11th ed. Oxford, United Kingdom ; New York, NY: Oxford University Press; 2018.